Vibro-acoustic sources in ground transportation

Ines Lopez Arteaga (1)(2)

(1) Eindhoven University of Technology, Department of Mechanical Engineering, Eindhoven, The Netherlands
(2) KTH Royal Institute of Technology, Marcus Wallenberg Laboratory for Sound and Vibration Research, Stockholm, Sweden

ABSTRACT

Long term exposure to ground transportation (road and rail traffic) noise is, after air pollution, the main environment-related health stressor in densely populated areas and compromises the quality of life and, indirectly, the life expectations of millions of people. At speeds up to 130 km/h in road traffic and up to 300 km/h in rail traffic the main source of noise is the tyre/road (respectively wheel/rail) interaction. In this paper the sound and vibration generation mechanisms due to tyre/road and wheel/rail interaction are discussed, focusing on the similarities and differences between the sound and vibration generation mechanisms in these two systems. This perspective is further extended to the discussion of contact force modelling and characterization methods in both road and rail traffic systems.

1 INTRODUCTION

Ground transportation noise is becoming an increasingly big problem in densely populated areas. This noise consists mainly of road and rail transportation noise. For road transportation tyre/road noise is the dominating noise source for constant driving speeds of 40 km/h and higher (Sandberg and Ejsmont 2002) for combustion engines and for all urban speeds in the case of electric vehicles. On the other hand for rail transportation, wheel/rail rolling noise is the main source of noise on open line (Thompson 2008).

Rolling noise of road and rail vehicles is very similar in nature, since both originate in vibrations caused by roughness-induced dynamic contact forces. In this paper the sound and vibration generation mechanisms due to tyre/road and wheel/rail interaction are discussed, focusing on the similarities and differences between the sound and vibration generation mechanisms in these two systems. In essence the source of noise is the dynamic contact forces caused by the (combined) surface roughness and, therefore, this paper focusses on discussing modelling and characterization of contact interaction.

2 FROM SURFACE ROUGHNESS TO SOUND GENERATION

2.1 Background

Ground transportation is based on rolling contacts due to their inherent low resistance to motion. However due to the surface roughness of the elements in contact, dynamic forces are generated during the rolling motion. These forces generate vibrations of the structures in contact and these vibrations lead to noise. The frequency of the excitation force is related to the wavelength of the surface roughness through the vehicle speed:

$$f = \frac{V}{\lambda}, \tag{1}$$

where f $[Hz]$ is the frequency, λ $[m]$ the wavelength and V $[m/s]$ the vehicle speed. This relationship is fundamental to understanding the dynamic response to rolling excitation and the negative effects associated to it as is schematically shown in Figure 1 (Lundberg 2016).

Very long wavelengths lead to low frequency excitation which, in case of coincidence with structural resonances, might lead to structural durability problems and high rolling resistance in tyres. For shorter wavelengths, comfort-related aspects such as vibrational disturbance and structure borne sound problems may appear. Even shorter wavelengths are usually accompanied by direct sound radiation from the rolling object or the supporting structure. Although the basic mechanism of roughness-induced vibrations is the same for tyre/road and wheel/rail interaction, there are significant differences in the contact, dynamic response and sound radiation mechanisms that are discussed in the following subsections.
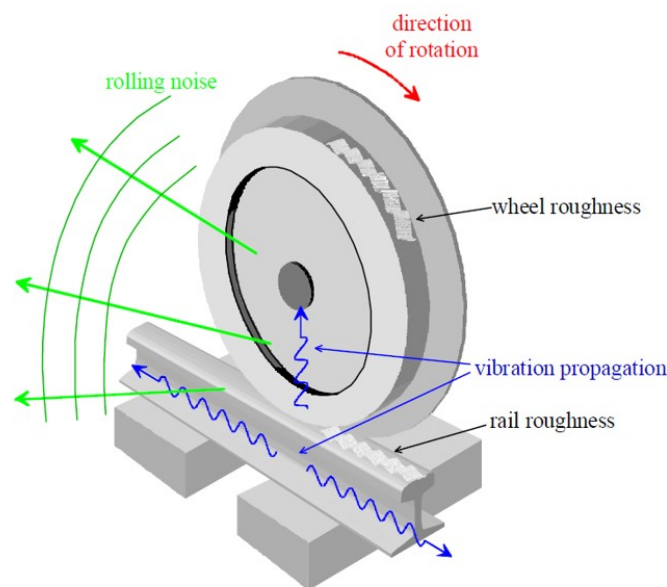
2.2 Particularities of wheel/rail noise

For rail vehicles the combined surface roughness of wheel and rail excites vibrations in both systems as shown in Figure 2 (Kuijpers 2005).
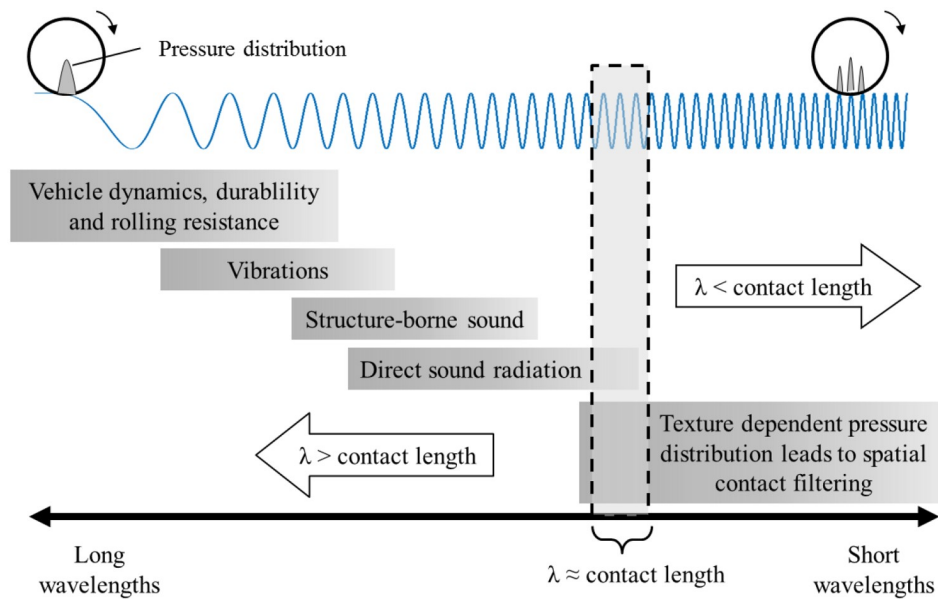
Source: Lundberg, PhD Thesis, 2016

Figure 1: Relation between surface texture wavelength and vibroacoustic aspects caused by rolling excitation.


Source: Kuijpers, 2005

Figure 2: Wheel/rail noise generation.

Both wheel and rail are efficient sound radiators in a broad frequency range and therefore the roughness-induced vibrations lead partly to noise and are partly transmitted to the sleepers which in turn radiate sound as well. The vibration energy of the wheels is concentrated around the eigenmodes of the wheel, generally above 1500 Hz. The rail radiates broadband sound in the frequency region 250-1250 Hz, while the sleepers are the main contributors to the total pass-by noise at low frequencies, below about 400 Hz. The structural damping of railway wheels is very low, which means that all vibration modes excited will easily reach relatively large vibration amplitudes at their corresponding resonance frequencies and, since the structural wavelengths are larger than the acoustic wavelengths for most frequencies of interest, radiate sound efficiently. On the other hand the track, unlike the road in tyre/road noise, is a major contributor to railway noise and the contact forces and the track response to these forces strongly depend on its dynamic properties, which are determined by: the rail properties, sleeper and rail pad properties and ballast properties.

2.3 Particularities of tyre/road noise

When a tyre rolls on a rough surface tyre vibrations are excited due to two main effects: the impacts caused by the tread blocks entering and exiting the contact area and the higher frequency excitation of the roughness wavelengths of the order of the tread block size within the contact area. This is schematically illustrated in Figure 3(a)-(b). As the tread blocks travel along the contact length, they are compressed by the road roughness asperities and the generated forces are transmitted to the tyre belt (see Figure 3(b)). The contact forces cause
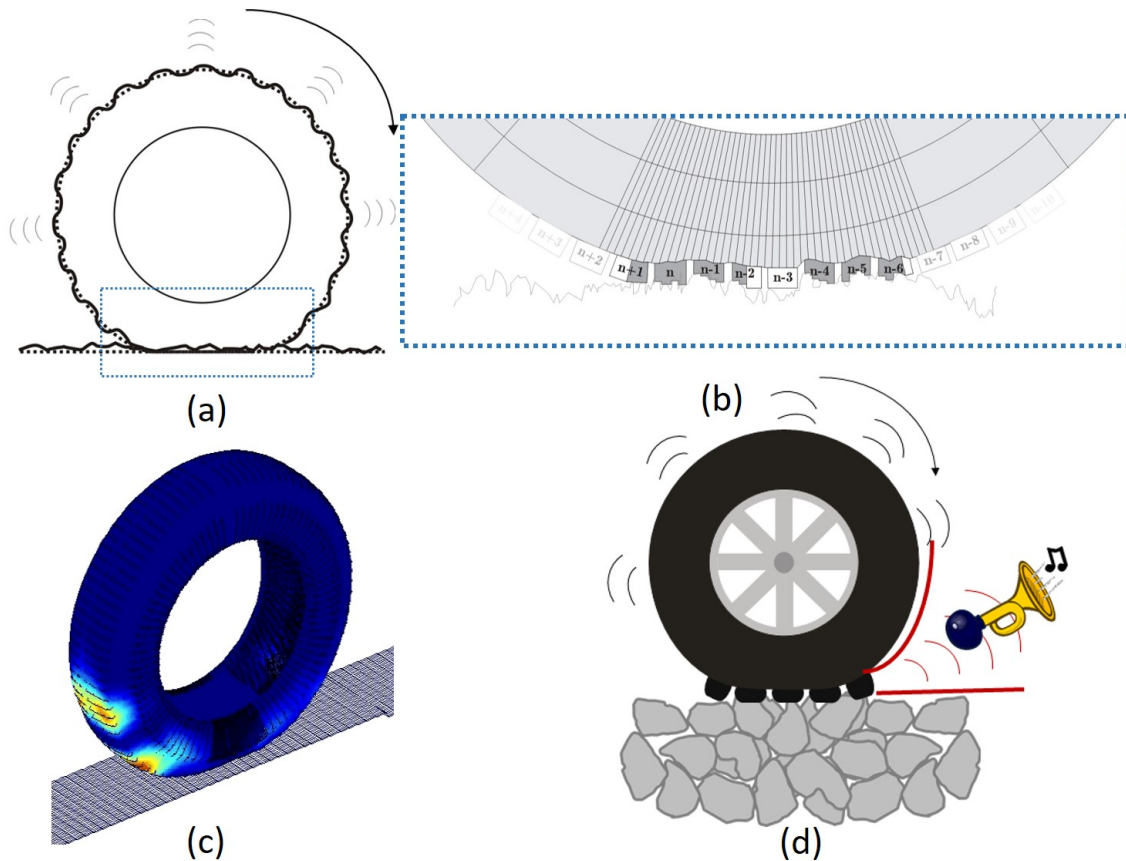
Source: Figure partly taken from (Boere et al. 2014)

Figure 3: Overview of tyre/road sound generation: (a) Schematic view of tyre on rough road, (b) Detailed view of interaction between tread blocks and road surface asperities, (c) Tyre vibrations due to road roughness excitation, (d) Sound amplification through the horn effect.

the tyre to vibrate as shown in Figure 3(c). Unlike vibrations in train wheels, elastic waves in tyres decay strongly as the distance to the contact area increases, which means that tyres themselves do not act as loudspeakers, as is the case for train wheels. In the case of tyre/road noise, the sound amplification is due to the horn effect as illustrated in Figure 3(d). The wedge at the leading edge of the tyre/road contact acts as a loudspeaker that can provide amplifications of the order of 30dB. Therefore road properties have a crucial influence on tyre/road noise. On the one hand road texture provides the excitation that makes the tyre vibrate and, on the other hand, a road with low acoustic absorption will greatly amplify the sound generated at the tyre/road contact. This inevitably leads to the conclusion that a smooth road with high sound absorption properties should greatly reduce tyre/road noise, as is the case (Sandberg and Ejsmont 2002).

2.4 General modelling approach

The general modelling approach for vibro-acoustic predictions of wheel/track and tyre/road interaction is schematically given in Figure 4, where $\mathbf{f}(t,\Omega), \hat{\mathbf{f}}(\omega,\Omega)$ are the force vectors in time and frequency domain respectively, $\mathbf{G}(t,\Omega)$ is a matrix of Green's functions of the interacting subsystems, $\mathbf{Y}(\omega,\Omega)$ is the matrix of mobilities of the interacting subsystems, ω rad/s is the temporal frequency and Ω rad/s is the rotational velocity of the wheel/tyre. This approach has been exploited by several authors in both the road and railway noise communities, where some works include the influence of the rotational velocity on the system response (see for example Pieringer, Baeza, and Kropp 2015, Lopez et al. 2007, Lopez-Arteaga 2011) and others do not (see for example Nordborg 2002, O'Boy and Dowling 2009).

$\mathbf{f}(t)$ → Fourier Transform → $\hat{\mathbf{f}}(\omega)$ → Linear dynamic models of interacting bodies

(Non-linear) contact model ← $\mathbf{G}(t,\Omega)$

Surface roughness

$\mathbf{Y}(\omega,\Omega)$ → Wheel/Tyre response → Sound radiation
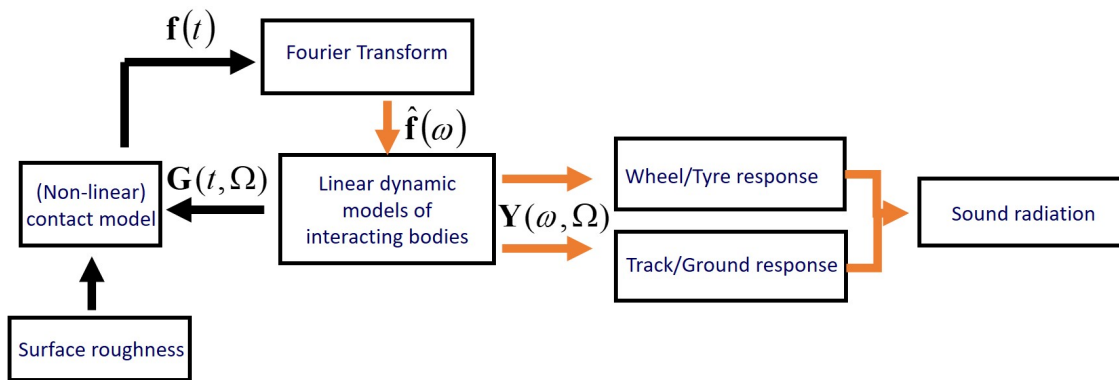
Track/Ground response

Figure 4: General modelling approach.

The idea behind the approach presented in Figure 4 is to separate the linear and nonlinear parts of the dynamic behavior of the system. For vibro-acoustic modelling it is reasonable to assume that the response of wheel/tyre and track/road is linear and can be described by Green's functions and mobilities. Which means that their response to the contact forces can be computed in the frequency domain. On the other hand, in order to account for the non-linear effects associated to the dynamic changes in the effective contact area caused by the surface roughness, the contact forces should be calculated in the time-domain. This leads to a two-step procedure where the contact forces are calculated in the time domain, considering the responses of the interacting structures through their Green's functions and with the (combined) roughness of the structures as input. In a second step, the contact forces are transformed to the frequency domain and the response of the interacting structures is obtained based on pre-calculated mobilities. This approach is computationally efficient, since the time consuming time-domain integration is performed with a relatively small model, including only the Green's functions for the parts of the structures that are potentially in contact.

Although this general approach is applied to both road and railway noise there are differences in how the interacting structures and the contact interaction are modelled and in the challenges involved. For wheel/track interaction wheel dynamics are modelled either as rigid body (when the track response is the main interest) or applying modal superposition of modes obtained from Finite Element (FE) models, which is a straightforward procedure. Track dynamics are more complex to describe due to relatively large amount of parameters that influence the response of the track as mentioned in Section 2.2 (see Thompson 2008). The contact is often modelled as a point contact (see for example Remington 1987, Nordborg 2002) applying Hertzian contact theory to determine the (nonlinear) contact stiffness and a filter to the combined roughness data in order to include the filtering effect of the contact patch (see Thompson 2008). This approach offers a limited description of the influence of the combined roughness on the contact forces as is further discussed in Section 3.

Regarding tyre/road interaction, the road is mostly modelled as an infinitely rigid surface and influences the sound generation through surface roughness and its sound absorption properties. Furthermore, tyres are complex structures, built of wires, cloth and several different rubber compounds, making accurate tyre modelling a hard task. A number of analytical models have been proposed in the literature such as plate models (Larsson and Kropp 2002) and cylindrical shell models (Pinnington 2006). Although analytical models have proved to be valuable to study the general dynamic behavior of tyres, they are difficult to use in the tyre design process. On the other hand full FE models are too complex and time consuming. The alternative that has won in popularity in recent years is the Waveguide Finite Element Method (WFEM) (Nilsson 2004), where the cross-section of the tyre is modelled using finite element (FE) and the vibration field in the circumferential direction is represented using waveguides. The second complexity factor in tyre/road noise is solving the contact problem between tyre and road. The size of the contact area depends on the load and the dynamic properties of the tyre and varies during rolling due to the road waviness and vehicle dynamics. Furthermore, the real contact area depends on the surface roughness of the road and is much smaller than the apparent contact area. Accurately predicting and measuring the 3-dimensional contact forces at the contact area is a challenging task that is further discussed in Section 4.

Summarizing, it is clear from the discussion in this and the previous section that a good understanding, accurate modelling and accurate measurements of rolling contact forces and the role of surface texture is key to the prediction and mitigation of transportation noise. Therefore in the following sections some detailed aspects of wheel/rail and tyre/road contact are discussed.

3 MODELLING ROUGHNESS-RELATED NONLINEARITY IN WHEEL/RAIL CONTACT

3.1 Background

Wheel/rail contact interaction is often simplified to a single contact point that moves along a line representing the combined wheel and rail roughness (Thompson 2008). Assuming full compression of this combined roughness, Hertzian contact theory can be applied to derive the resulting contact force. The Hertzian contact stiffness is usually linearized around the equilibrium position corresponding to the static vehicle load and applied to both time- and frequency-domain wheel/track interaction modelling (Nordborg 2002, Wu and Thompson 2000, (Remington 1976). Regardless of the linearization step, Hertzian theory is based on three assumptions: smooth surfaces, elliptic contact area and the assumption that one line of combined roughness represents the three-dimensional roughness profile within the contact area of 0.8 to 2.5 cm^2 (Remington 1976). In practice, short roughness wavelengths smaller than the contact dimensions should be filtered in order to achieve realistic predictions in the high frequency range and the correlation of the roughness profile in the longitudinal and lateral direction influences the level of excitation (Pieringer, Kropp, and Thompson 2011).

Over the years, methods to increase the accuracy of the effective combined roughness profile have been developed, such as two- and three-dimensional elastic foundation models (Thompson 2008). These models rely on a pre-calculation of the (non-linear) contact stiffness and the effective combined roughness profile and solve the wheel/track interaction problem as a point contact problem. In (Pieringer, Kropp, and Thompson 2011) detailed three-dimensional contact modelling is included in the time-domain wheel/track dynamic interaction model, eliminating all simplifications related to the point contact assumption.

Although time-domain models of wheel-track interaction including three-dimensional contact modelling enable predictions of high accuracy, they entail a high computational cost and require complete three-dimensional roughness data for the total length along the rolling direction. Therefore in (Lundberg, Nordborg, and Lopez Arteaga 2016) a method is proposed that captures the roughness- and shape-induced non-linear effects on both contact stiffness and contact filtering, while keeping the single-point contact approach, leading to a low computational cost and a limited amount of input roughness data. This method is a further development of the contact model developed and validated in (Lundberg et al. 2015) for the general case of steel-steel rolling contacts. A summarized description is provided in the following subsections.

3.2 Nonlinear contact stiffness and filtering

In the rolling contact modelling approach proposed in (Lundberg et al. 2015) and further developed in (Lundberg, Nordborg, and Lopez Arteaga 2016), the point contact force is given by

$$F_c = k_c(r - \tilde{h}), \quad r - \tilde{h} > 0, \tag{2}$$

where k_c [N/m] is the space dependent contact stiffness, r [m] is the relative displacement between the wheel and the rail and $\tilde{h}$ [m] is the state dependent (filtered) gap. The original gap function $h(x,y)$ contains all the information needed to describe the shape and roughness of the contacting bodies (Lundberg, Nordborg, and Lopez Arteaga 2016).

The pre-calculation of the state-dependent functions is performed by three-dimensional contact modelling which requires the generation of small size surface textures with high spatial resolution. In (Lundberg, Nordborg, and Lopez Arteaga 2016) two combinations of wheel-rail contact are considered: low-roughness contact and high roughness contact (see Figure 5). A three-dimensional elastic contact model based on Boussinesq static contact-theory is used in which a grid of rectangular cells covers the contact area. The influence coefficients C_{ij} relate the deformation at cell i to the pressure at cell j:

$$\mathbf{Cp} = \mathbf{r} - \mathbf{h}, \tag{3}$$

where matrix $\mathbf{C}$ contains the influence coefficients C_{ij}, the elements of vector $\mathbf{h}$ are the gaps between wheel and rail in each cell, the elements of vector $\mathbf{p}$ are the corresponding pressures and vector $\mathbf{r}$ contains the relative displacements r between the contacting bodies. The numerical integration of the pressures obtained from Equation 3 over the total contact area leads to the resultant normal force

$$F_c = \sum \mathbf{p}S, \tag{4}$$

where S is the grid cell area within which a uniform pressure distribution is assumed.

3.2.1 State-dependent contact stiffness

The contact simulation procedure given by Equations (3) and (4) is used in a quasi-static manner starting at a value of zero compression and stepwise increasing the relative displacement in small steps. A value of the compression
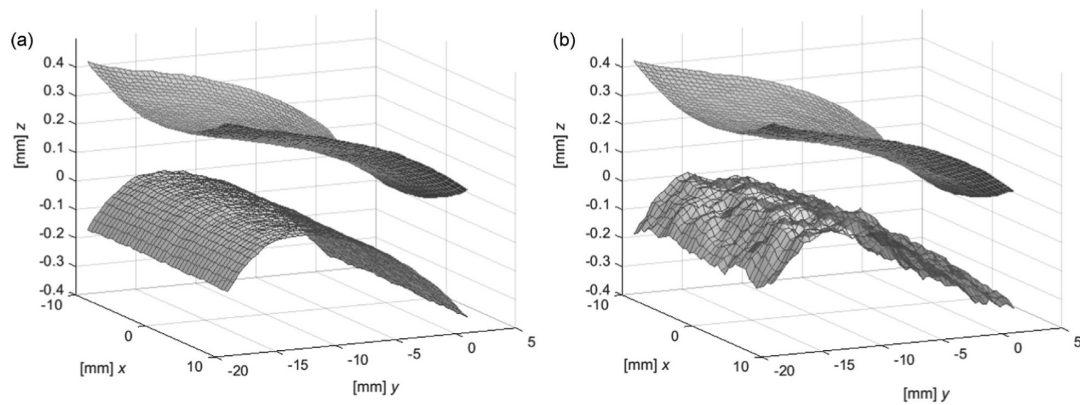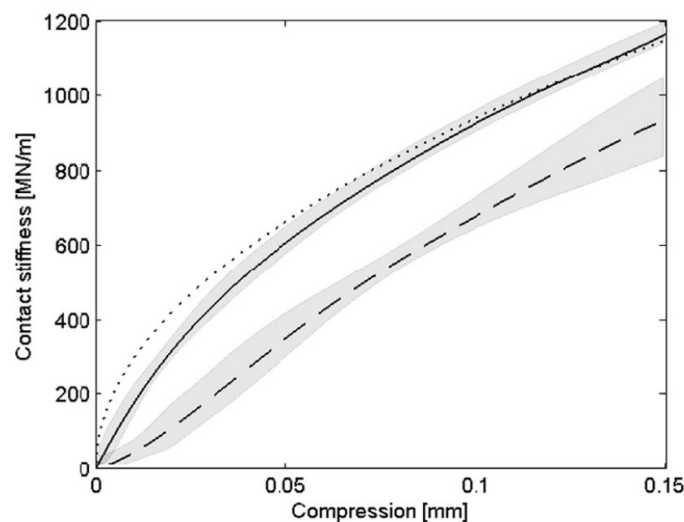
Source: Lundberg et al., 2016

Figure 5: Wheel and rail geometry for three-dimensional contact computations: (a) low roughness contact and (b) high roughness contact.

and the corresponding force is registered for each computational step (i) and the contact stiffness is estimated as

$$k_{c,i} = \frac{F_{c,i}}{r_i - h_n}, \tag{5}$$

where h_n is the gap value for the grid cell where the two bodies would first touch if they were brought together. This calculation is repeated for N surface samples, each with its unique reference gap value h_n, and the nonlinear relationship between compression and contact stiffness is obtained after ensemble averaging of the N computed arrays of stiffness values and polynomial curve fitting. The result is the state-dependent nonlinear contact stiffness k_c in Equation (2) and is plotted in Figure 6 for the two roughness profiles given in Figure 5, together with the Hertzian contact stiffness for comparison. Figure 6 clearly shows that the larger the amplitude of the combined
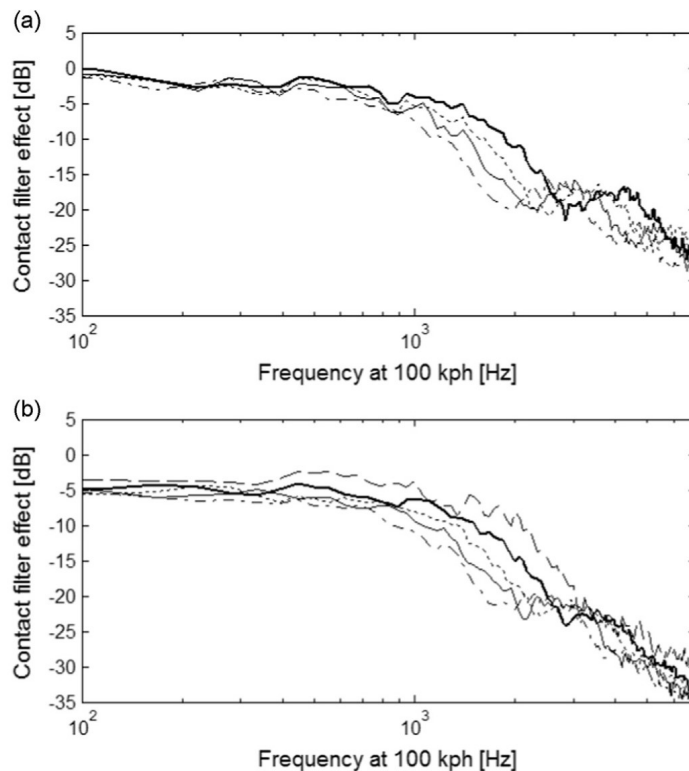

Source: Lundberg et al., 2016

Figure 6: Contact stiffness for low roughness contact (solid) and high roughness contact (dashed), with two standard deviations above and below the curve-fitted values (shaded), Hertzian contact stiffness as defined in (Wu and Thompson 2000) (dotted).

roughness profile the more the contact stiffness deviates from the Hertzian contact stiffness. For the same compression, an increase of the surface roughness amplitude leads to a smaller area of real contact and, therefore, a smaller contact force and a contact stiffness significantly lower than the Hertzian contact stiffness.

3.2.2 State-dependent contact filtering

During rolling the contact area changes due to dynamic load variations and so does the spatial filtering, which implies that the spatial filtering is nonlinear with respect to the vertical compression. In order to derive the state-dependent contact filters, the static load (resultant contact force F_c) is imposed and the relative displacements along the contact length in the rolling direction are calculated from Equations (4) and (3). The filter effect is calculated subtracting the average relative displacement for the apparent contact length from the calculated sequence of relative displacements. The procedure is repeated for N surface samples and the ensemble average is calculated to obtain the filter effect for the given static load. In Figure 7 the filter effect for the two combined roughness profiles considered and several static load values is shown. It can be seen that the contact filter spectra display
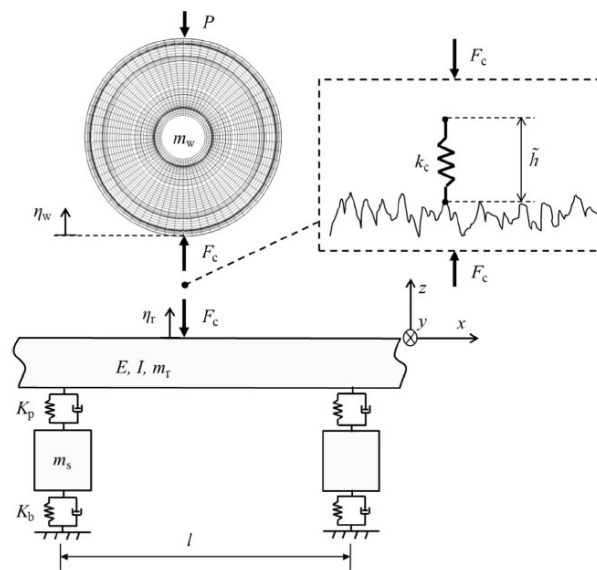

Source: Lundberg et al., 2016

Figure 7: Contact filter effect for static pre-loads 10kN (dashed), 25kN (thick solid), 45kN (dotted), 67.5kN (thin solid) and 100kN (dash-dotted) for (a)low roughness contact and (b) high roughness contact.

dips at frequencies corresponding to roughness wavelengths which are similar to the length of the apparent contact area. These dips seem to be more pronounced for the low roughness contact than for the high roughness contact, which is possibly explained by the fact that the contact length for the low roughness profile is well-defined as compared to the high roughness contact, leading to a more Hertzian-like pressure distribution. Furthermore, the high roughness contact leads to a larger contact filtering effect than the low roughness contact. A possible explanation is that, for the high roughness contact, parts of the wheel-rail material within the apparent contact area are not in contact leading to a reduced roughness-excitation. Although the filtering effect increases with increasing frequency (decreasing wavelength), it does not appear to be restricted to wavelengths shorter than (or of the order of) the contact dimensions.

The final step in the determination of the state-dependent contact filters is to fit a linear-phase Finite Impulse Response (FIR) filter on the sequence of gap values in the rolling direction for the total length of the investigated rolling contact (see Lundberg, Nordborg, and Lopez Arteaga 2016).

### 3.3 Wheel/rail interaction model and simulation results

The state-dependent contact stiffness and contact filter derived above are implemented in the wheel/track interaction model presented in (Nordborg 2002), and shown in Figure 8, to study the influence of state-dependent stiffness and filtering on the contact forces and rail vibration. The wheel/track interaction model includes elastic wave propagation in both wheel and rail. Parametric studies are performed, for two static load values and two

Source: Lundberg et al., 2016

Figure 8: Overview of wheel/track interaction model.

roughness levels, considering nonlinear, linear and Hertzian variants of the contact. In Figure 9 the effect of contact filtering is shown for nonlinear (dynamic) contact filtering, linear (static) contact filtering and for a Hertzian contact model by averaging the gap values over the nominal contact length. The reference is a Hertzian contact model without contact filtering. In general it can be concluded that state-dependent contact filtering leads to a
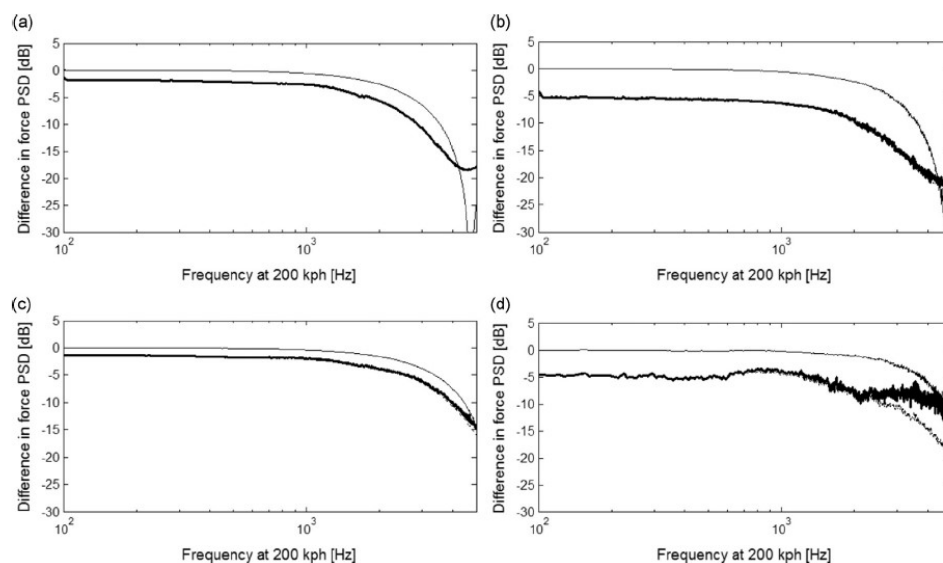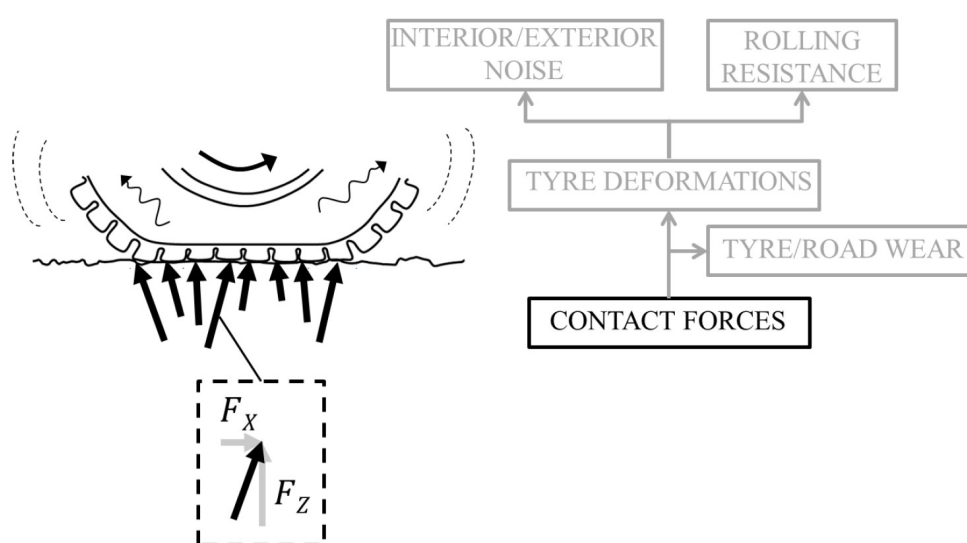

Source: Lundberg et al., 2016

Figure 9: Contact filter effect for vehicle speed 200kph and state-dependent contact model with nonlinear (dynamic) contact filtering (thick solid), state-dependent contact model with linear (static) contact filtering (dotted) and Hertzian contact model with filtering by averaging the gap-values over the contact length (thin solid). As reference the Hertzian contact model without contact filtering is used: (a) static load 67.5kN and low roughness excitation, (b) static load 67.5kN and high roughness excitation, (c) static load 25kN and low roughness excitation and (d) static load 25kN and high roughness excitation.

larger contact filtering effect than the Hertzian contact model with contact filtering by averaging over the contact length and that the effect is more pronounced for the higher roughness profile. Regarding the comparison between the linear (static) and nonlinear (dynamic) filtering, the largest differences are found for the low static loads and high roughness profile, reaching 8-10 dB for the vehicle speed of 200 kph. The influence of nonlinearities at lower vehicle speeds is however moderate (Lundberg, Nordborg, and Lopez Arteaga 2016).

4   UNDERSTANDING TYRE/ROAD ROLLING CONTACT INTERACTION

4.1   Background

The relatively low rigidity of rubber, together with its viscoelastic properties and the higher level of surface roughness of roads compared to metal-metal contacts leads to some fundamental differences in rolling contact conditions. In contrast to a railway wheel a tyre has the ability to transfer very high longitudinal and transverse forces between vehicle and road and to effectively mitigate the normal contact forces originating from the impact of the tread blocks on the road. This beneficial performance comes at the cost of a higher complexity of the rolling contact interaction. The bending and compression of the tyre when it goes through the contact patch give rise to longitudinal forces on the tread block which in the impact phase act in the tyre rolling direction and in the release phase act in the direction of the vehicle. For perfectly free rolling tyres, these contributions balance each other and lead to a zero net longitudinal force. However, in all real rolling conditions there is always a net longitudinal acceleration or braking present in the tread-block/road contact although it can be low in magnitude if it is present only to overcome the rolling resistance of the vehicle. As shown in Figure 10 the contact forces generated in the rolling process lead to several unwanted effects such as: tyre wear, rolling resistance and noise. Understanding the generation of tyre/road contact forces is the key to a better control of these effects. The vast majority of tyre/road


Source: Lundberg, PhD Thesis, 2016

Figure 10: Contact forces in the tyre/road interface generate interior and exterior noise as well as rolling resistance and wear.

contact interaction models for vibro-acoustic prediction purposes that can be found in the literature consider only vertical contact forces (Boere et al. 2014, O'Boy and Dowling 2009, Winroth, Andersson, and Kropp 2014) and disregard the longitudinal and transversal (friction) forces. This is partly due to the fact that the rubber/road contact interaction processes that ultimately lead to the friction force are still not fully understood and there is, therefore, a need for empirical data. Although there are several measurement methods that measure contact forces on complete tyres (Pacejka 2012), the contact forces are indirectly derived from forces measured in the wheel hub, which is valuable for global validation of tyre models but provides no information on the interaction between tyre-tread and road roughness within the contact. Several works can be found where methods to measure sliding friction between a single tread block and a substrate, excluding the complete tyre structure, are presented (see for example Van Der Steen, Lopez, and Nijmeijer 2011 and Rantonen, Tuononen, and Sainio 2012). However few methods can be found that attempt to measure contact forces between a tread block and a substrate in rolling conditions. In (Liu, Sutcliffe, and Graham 2012) a high speed rolling test rig is developed which is used to measure the normal and longitudinal rolling contact forces between a single tread block and a single stone asperity and more recently a compact internal drum (CID) measurement set-up is proposed, where the interaction between a tread block and an asphalt substrate is studied for representative impact and release conditions (Lundberg, Kari, and Lopez Arteaga 2017).

4.2   Compact Internal Drum (CID) set-up

The compact internal drum (CID) test rig (see Figure 11) is developed for measurements of the three contact force components generated in the impact and release phase of a tyre tread block in rolling contact with a substrate. The design of the test rig is such that realistic impact and release angles for the tread block–substrate contact are

provided and force measurements at high rolling speeds with a high signal-to-noise ratio are enabled. It is suitable for detailed investigations of the influence of rubber tread block and substrate characteristics on the contact forces, since both the substrate as well as the sample tread block are fully interchangeable. The core of the measurement
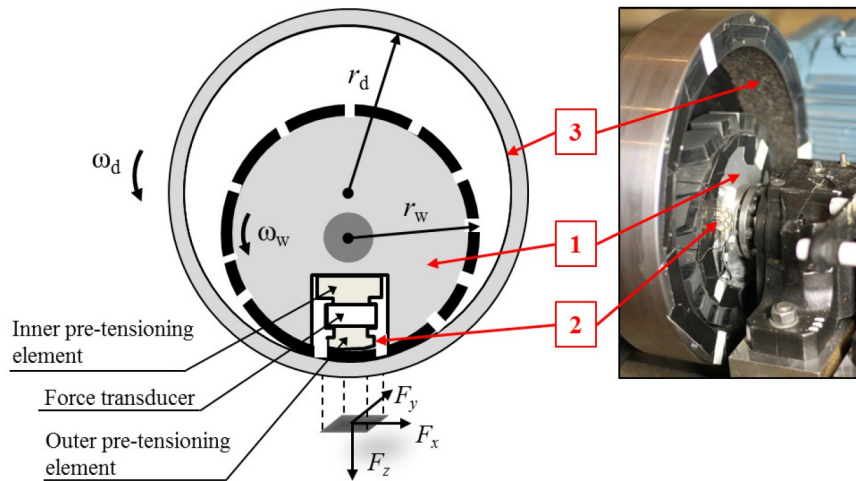
Source: Lundberg et al., 2017

Figure 11: The core of the test rig consists of a solid metal wheel (1) within which a force link (2) including a tread block sample is embedded. In test rig operation, the solid metal wheel rolls on the inner surface of a drum (3), which is covered by an interchangeable sample substrate

test rig is a solid metal wheel (1) with an embedded force link (2), consisting of an inner pre-tensioning element, a three-axial piezoelectric force transducer and an outer pre-tensioning element. The force link is positioned and radially fixed in the solid metal wheel which has been prepared by cutting out a section which is slightly larger than the force link itself, such that the force link is fully decoupled from the solid wheel in the tangential direction. A strip of tread rubber is cut out of a truck tyre retread material (Lundberg, Kari, and Lopez Arteaga 2017) and glued to the circumference of the solid metal wheel, ensuring that one of the tread blocks is centered on the outer pre-tensioning element of the force link. The contact forces are measured on the sample tread block when the wheel rolls on the inner surface of a drum, which is covered by an interchangeable sample substrate (3). The equivalent radius r_e formed by the outer radius of the solid wheel r_w and the inner radius of the drum r_d determines the impact and release angle for the tread block. By carefully choosing the wheel and drum radii, impact and release angles very similar to those found at the tyre/road contact can be realized. An electric motor generates the driving torque that drives the inner wheel and is transmitted to the drum through the friction forces between rubber blocks and the substrate mounted on the drum. Additionally, a breaking torque can be applied to the shaft in which the drum is mounted. The rotational velocities of the solid wheel ω_w and the drum ω_d are measured with optical sensors and used to determine the longitudinal slip

$$s_x = \frac{v_w - v_d}{v_d}, \tag{6}$$

where $v_w = r_w \omega_w$ is the velocity of the solid wheel and $v_d = r_d \omega_d$ is the velocity of the drum. The longitudinal slip s_x is needed in order to quantify the amount of breaking or acceleration during the measurements. See (Lundberg, Kari, and Lopez Arteaga 2017) for detailed information on the CID set-up.

4.3 Experimental results
The dynamic contact forces in the vertical, longitudinal and transversal direction are measured for an asphalt surface with maximum stone size 4mm (see Figure 12). Measurements for a rolling velocity of v_d of 3.6 m/s and a static load of 70 N are performed with and without driving torque (Figure 13) and with driving torque and constant acceleration conditions simulated by applying a breaking torque (Figure 14).

Both figures show the resulting contact forces and the friction coefficient

$$\mu_x = \frac{F_x}{F_z}, \tag{7}$$

with F_x the longitudinal force and F_z the transversal force. The friction coefficient is only defined when the tread block is in contact with the substrate.

(a)

(b)
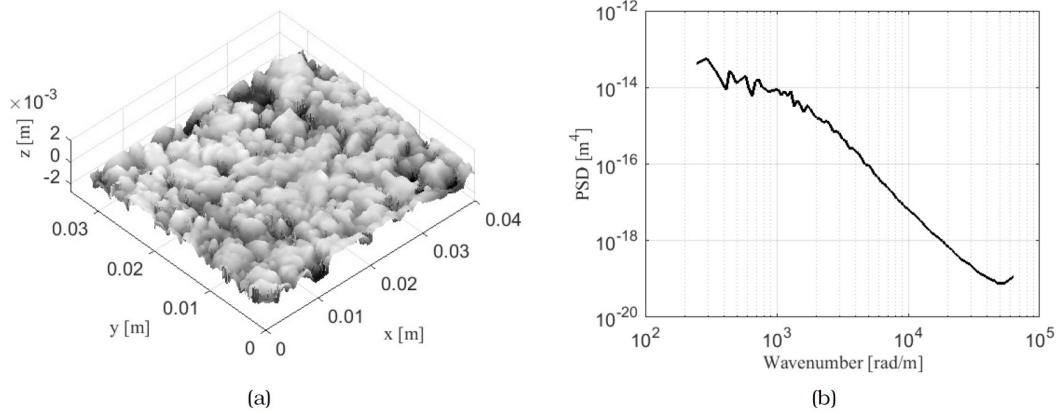
Source: Lundberg et al., 2017

Figure 12: Surface properties of NCC Repasfalt / Vialit Reaktiv Asphalt, maximum stone size 4mm. (a) Surface topography using optical fringe projection (b) Power Spectral Density (PSD) of the surface roughness
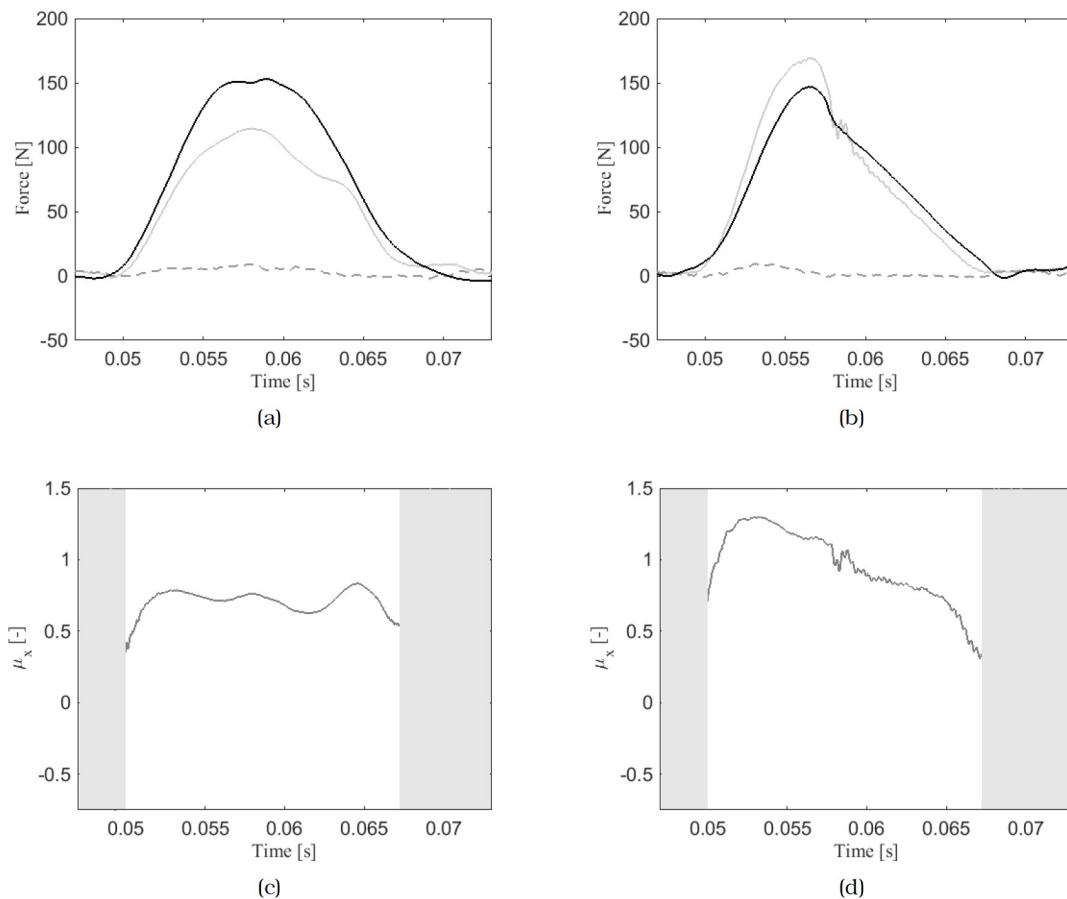

(a)

(b)

(c)

(d)
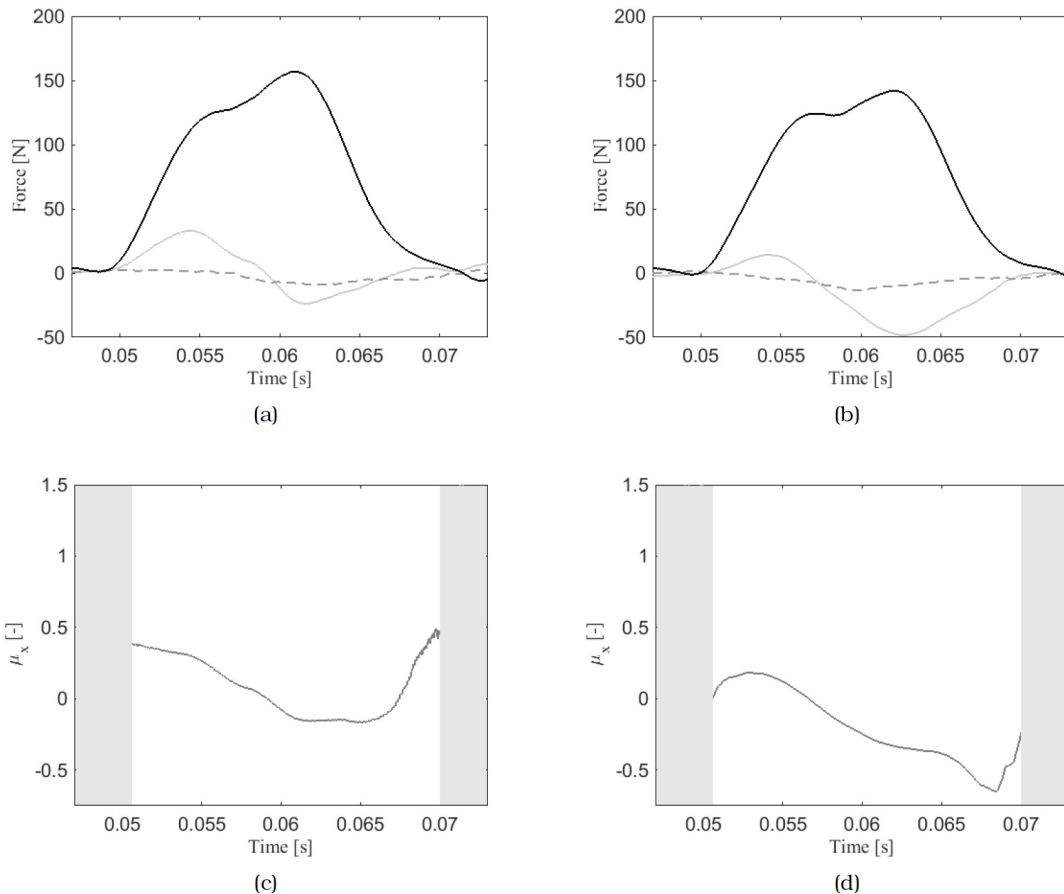
Source: Lundberg et al., 2017

Figure 13: Measured longitudinal (solid grey), transverse (dashed) and vertical (solid black) contact forces for rolling velocity 3.6 m/s and static load 70 N; (a) with driving torque; (b) without driving torque; (c) longitudinal friction coefficient with driving torque during the time of contact; (d) longitudinal friction coefficient without driving torque during the time of contact.

The vertical compression of rubber leads to vertical compressive stresses as well as longitudinal shear stresses directed towards the center of the contact area. A sinusoidal-like longitudinal force history is found since the tread

block is deformed towards the leading edge at impact and subsequently deformed towards the trailing edge in the release phase. In Figure 13(a), this sinusoidal-like character is distorted by a superimposed shear force directed towards the leading edge which correspond to the force required to overcome the rolling losses of the test rig and maintain a constant velocity. The force history immediately after the driving torque has been removed is presented in Figure 13(b), where the superimposed longitudinal shear force is directed towards the trailing edge. This sinusoidal-shaped force history is found in numerous experimental investigations of the longitudinal forces on complete rolling tyres (see for example Van Der Steen et al. 2011) as well as in the investigation of a single tread block in rolling contact performed by (Liu, Sutcliffe, and Graham 2012). Due to the asymmetry of the tread block shape (leading and trailing edge are not perpendicular to the direction of travel), also a transverse shear force is measured, although it is small compared to both the vertical and the longitudinal force components.

Source: Lundberg et al., 2017

Figure 14: Measured longitudinal (solid grey), transverse (dashed) and vertical (solid black) contact forces for rolling velocity 3.6 m/s and static load 70 N; (a) with driving torque and braked drum ($sx = 0:038$); (b) with driving torque and heavily braked drum ($sx = 0:100$); (c) longitudinal friction coefficient with driving torque and braked drum during the time of contact; (d) longitudinal friction coefficient with driving torque and heavily braked drum during the time of contact.

Constant acceleration is simulated by the application of a braking torque to the drum and simultaneously a driving torque generated by the electric motor sufficient to maintain a constant rolling velocity. In Figure 14(a)-(b), the resulting contact forces are presented for simulated constant acceleration at the rolling velocity 3.6 m/s. In this case, as one would expect, the longitudinal force is positive for the complete contact length and significantly larger than before. For the heavy breaking conditions the longitudinal force is larger than the normal force, which leads to a friction coefficient larger than one, as shown in Figure 14(d). This result is in agreement with experimental results presented by (Van der Steen 2010).

The capability of the test rig to generate useful results is assessed by presenting results for both free rolling and accelerating condition at different rolling velocities and different static vertical pre-loads. The test rig thus provides

results which contribute to the understanding of tyre/road interaction and can be used as input to modelling-based development of both tyres and roads aiming for improved handling, safety, energy efficiency, comfort and acoustic performance.

5   CONCLUSIONS

This paper discusses the similarities and differences in the sound generation process of rolling noise for road and rail vehicles. It is shown that in essence the force and vibration generation mechanisms are similar and the both problems can be modelled following analogous approaches. Nevertheless, the specific contact interaction conditions and the sound radiation mechanisms are very different. Since the key to minimizing rolling noise generation are the contact forces, this paper further explores rolling contact interaction from the modelling perspective for wheel/rail interaction and from the experimental perspective for tyre/road noise.

ACKNOWLEDGEMENTS

REFERENCES

Boere, Stijn, Ines Lopez Arteaga, Ard Kuijpers, and Henk Nijmeijer. 2014. "Tyre/road interaction model for the prediction of road texture influence on rolling resistance." *International Journal of Vehicle Design* 65 (2-3): 202–221.

Kuijpers, Ard. 2005. "Towards silent tracks and roads: beating the roughness." *Proc. ForumAcusticum Budapest:* 1159–1164.

Larsson, K, and W Kropp. 2002. "A high-frequency three-dimensional tyre model based on two coupled elastic layers." *Journal of sound and vibration* 253 (4): 889–908.

Liu, F, MPF Sutcliffe, and WR Graham. 2012. "Prediction of tread block forces for a free-rolling tyre in contact with a rough road." *Wear* 282:1–11.

Lopez, I., R. Blom, N. Roozen, and H.Nijmeijer. 2007. "*Modelling vibrations on deformed rolling tyres - a modal approach.*" *Journal of Sound and Vibration* 307 (3-5): 481–494.

Lopez-Arteaga, I. 2011. "*Green's functions for a loaded rolling tyre.*" *International Journal of Solids and Structures* 48 (25-26): 3462–3470.

Lundberg, Oskar E. 2016. "On the influence of surface roughness on rolling contact forces." PhD diss., KTH Royal Institute of Technology.

Lundberg, Oskar E, Svante Finnveden, Stefan Björklund, Mikael Pärssinen, and Ines Lopez Arteaga. 2015. "A nonlinear state-dependent model for vibrations excited by roughness in rolling contacts." *Journal of Sound and Vibration* 345:197–213.

Lundberg, Oskar E, Leif Kari, and Ines Lopez Arteaga. 2017. "A compact internal drum test rig for measurements of rolling contact forces between a single tread block and a substrate." *Measurement* 103:370–378.

Lundberg, Oskar E, Anders Nordborg, and Ines Lopez Arteaga. 2016. "The influence of surface roughness on the contact stiffness and the contact filter effect in nonlinear wheel–track interaction." *Journal of Sound and Vibration* 366:429–446.

Nilsson, Carl-Magnus. 2004. "Waveguide finite elements applied on a car tyre." PhD diss., Farkost och flyg.

Nordborg, Anders. 2002. "Wheel/rail noise generation due to nonlinear effects and parametric excitation." *The Journal of the Acoustical Society of America* 111 (4): 1772–1781.

O'Boy, DJ, and AP Dowling. 2009. "Tyre/road interaction noise—Numerical noise prediction of a patterned tyre on a rough road surface." *Journal of Sound and Vibration* 323 (1): 270–291.

Pacejka, H. 2012. *Tire and Vehicle Dynamics.* Elsevier Ltd,

Pieringer, A., W. Kropp, and D.J. Thompson. 2011. "Investigation of the dynamic contact filter effect in vertical wheel/rail interaction using a 2D and a 3D non-Hertzian contact model." Proceedings of the 8th International Conference on Contact Mechanics and Wear of Rail / Wheel Systems, Florence, 2009, *Wear* 271 (1): 328–338. ISSN: 0043-1648. doi:http://dx.doi.org/10.1016/j.wear.2010.10.029. http://www.sciencedirect.com/science/article/pii/S0043164810003637.

Pieringer, Astrid, Luis Baeza, and Wolfgang Kropp. 2015. "Modelling of railway curve squeal including effects of wheel rotation." In *Noise and Vibration Mitigation for Rail Transportation Systems,* 417–424. Springer.

Pinnington, RJ. 2006. "A wave model of a circular tyre. Part 1: belt modelling." *Journal of Sound and Vibration* 290 (1): 101–132.

Rantonen, Marko, Ari Juhani Tuononen, and Panu Sainio. 2012. "Measuring stud and rubber friction on ice under laboratory conditions." *International Journal of Vehicle Systems Modelling and Testing* 7 (2): 194–207.

Remington, Paul J. 1976. "Wheel/rail noise—Part IV: Rolling noise." *Journal of Sound and Vibration* 46 (3): 419–436.

Remington, Paul J. 1987. "Wheel/rail rolling noise, I: Theoretical analysis." *The Journal of the Acoustical Society of America* 81 (6): 1805–1823.

Sandberg, Ulf, and Jerzy A Ejsmont. 2002. *Tyre/road noise reference book.* Informex, SE-59040 Kisa, Sweden.

Thompson, David. 2008. *Railway noise and vibration: mechanisms, modelling and means of control.* Elsevier.

Van der Steen, R. 2010. "Enhanced friction modeling for steady-state rolling tires." PhD diss., Eindhoven University of Technology.

Van Der Steen, R, I Lopez, H Nijmeijer, A Schmeitz, and B De Bruijn. 2011. "Experimental and numerical study of friction and braking characteristics of rolling tires." *Tire Science and Technology* 39 (2): 62–78.

Van Der Steen, R, Ines Lopez, and Henk Nijmeijer. 2011. "Experimental and numerical study of friction and stiffness characteristics of small rolling tires." *Tire Science and Technology* 39 (1): 5–19.

Winroth, Julia, PBU Andersson, and Wolfgang Kropp. 2014. "Importance of tread inertia and damping on the tyre/road contact stiffness." *Journal of Sound and Vibration* 333 (21): 5378–5385.

Wu, TX, and DJ Thompson. 2000. "Theoretical investigation of wheel/rail non-linear interaction due to roughness excitation." *Vehicle System Dynamics* 34 (4): 261–282.